4-1-2 Automatic Scaling of Echo Traces on Ionogram: An Attempt to Separate Propagation Modes

UEMOTO Jyunpei, KUBOTA Minoru, MARUYAMA Takashi, and ISHII Mamoru

Although algorithms for automatically scaling ionospheric reflective echoes on ionograms collected through ionosonde observations have long been developed to derive a vertical ionospheric electron density profile, the scaling performance of these existing algorithms have both merits and demerits due to the complexity of ionospheric reflective echoes. This paper summarizes the performance requirements of an automatic scaling algorithm that overcomes the limitations on existing algorithms, and discusses a scheme of automatically tagging the propagation modes of ionospheric reflective echoes as a key to developing such an algorithm.

Keywords
Ionosonde, Ionogram, Automatic scaling

1 Introduction

Ionosonde observations have been widely performed worldwide as a means of observing ionospheric electron density structures ever since related techniques were first established in the 1920s. It is no exaggeration to say that our present-day knowledge about the basic structure of ionospheric electron density was brought about by ionosonde observations. In recent years, ionosonde observations have been performed for monitoring ionospheric irregularities that adversely affect GPS, applying to physical values that are difficult to observe such as thermospheric neutral wind, and continue being one of the most effective means of observation in conducting ionospheric studies. Moreover, ongoing ionosonde observations are assuming greater importance in recent years as reported by Reference [1] on the relationship between long-term ionospheric variations and global warming as estimated from ionosonde observation data.

An ionosonde transmits radio waves toward the ionosphere while sweeping frequencies, and then measures the time (delay time) until the transmitted radio waves are reflected back to the ground by the ionosphere (Fig. 1 (a)). The observation data is normally represented in a diagram called an "ionogram" that expresses signal strength as a contour with the apparent altitude (*i.e.*, half the value of round-trip distance between the ground and reflecting point as calculated by multiplying delay time by speed of light c) being taken on the axis of ordinate, and frequency on the axis of abscissa (Fig. 1 (b)).

The curve pointed to by each arrow in Fig. 1 (b) designates an echo from the ionospheric *F*-region that reflects information about vertical height distributions of ionospheric electron density ($N(h)$ profile). Ionograms offer a very convenient information for understanding the overall structure of the ionospheric electron density. But since the group velocity of transmitted radio waves is a function of the ionospheric electron density and magnetic field, it is necessary to scale the frequency and delay time of reflective echoes sequentially, and then convert them into a $N(h)$ profile with the group velocity of propagation in plasma taken into account, in order to derive a $N(h)$ profile of numeric data like that shown in Fig. 2.

This means that the $N(h)$ profile would not

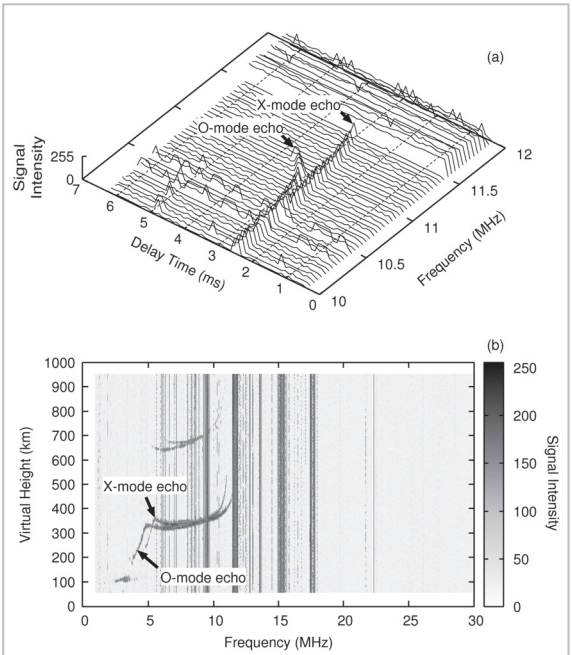

Fig.1 *(a) 3D representation of ionogram observation data, Each individual line represents the measured amplitude along the delay time at each frequency.*
(b) Ionogram collected in Okinawa at 11:45 on April 4, 2005 JST (JST = UT + 9 hrs), Traces in the virtual height range between 200 to 600 km pointed to by the arrow marks designate reflective echoes from the ionospheric F-region.

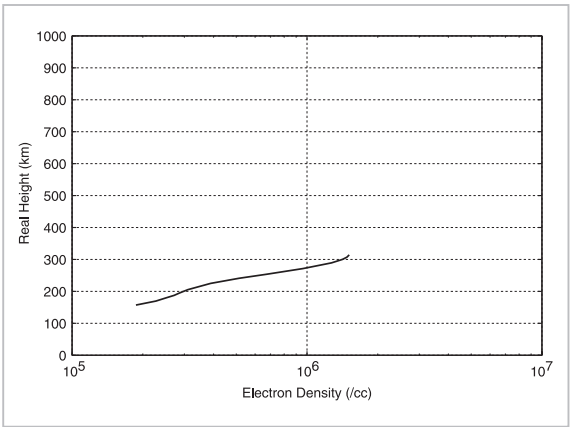

Fig.2 *N(h) profile derived from manually scaling the O-mode reflective echo on the ionogram shown in the Fig.1(b)*

be derived from ionograms without scaling reflective echoes. The manual scaling is a laborious and complex job, and proficient skills are required to ensure scaling accuracy. For this reason, algorithms for automatically scaling ionospheric reflective echoes have long been developed (as mentioned in References [2]–[6]). Achieving automatic reflective echo scaling capability would not only be of vital importance to implementing real-time alerts regarding ionospheric electron density irregularities, which could threaten the stable usage of satellite communications systems such as GPS, but also greatly instrumental in probing the relationship between long-term ionospheric variations and global warming, a topic on which more light has been shed in recent years. Yet, automatic reflective echo scaling has been made difficult by undesired noise contained in the ionograms, a partial lack of reflective echoes, the complex geometries of reflective echoes, superimposition of reflective echoes of multiple propagation modes, and other factors; consequently, existing algorithms have both merits and demerits in terms of scaling performance.

This paper summarizes the requirements of an automatic reflective echo scaling algorithm, and discusses a scheme of automatically tagging the propagation modes of ionospheric reflective echoes as a key to developing such an algorithm.

2 Basic principles of ionosonde observations

As mentioned in Chapter **1**, the basic principle of ionosonde observations is measuring the time delay of radio waves transmitted toward the ionosphere while sweeping frequencies. Assuming the transmitted radio wave has frequency f, with $d(f)$ denoting the time delay and $h'(f)$ the apparent vertical height, the relationship between f, $d(f)$, and $h'(f)$ can be expressed in an equation as follows:

$$h'(f) = \frac{c}{2} d(f) = \int_0^{h_r} \frac{c}{V_g} dh = \int_0^{h_r} n' dh \quad (1)$$

where, h denotes the vertical height from the ground, h_r the actual vertical height of the reflecting point of the transmitted radio wave,

and V_g the group velocity. The coefficient of 1/2 is for round-trip distance. Here, $n' = (c/V_g)$ is called a group refractive index and can be expressed in an equation using refractive index n in the plasma and transmitting frequency f as follows:

$$n' = n + f\frac{\partial n}{\partial f} \tag{2}$$

Refractive index n is a function of electron density $N(h)$, magnetic field strength $B(h)$, and angle θ between the magnetic field and propagation vector of the transmitted radio wave, and can be expressed in an equation as follows:

$$n = \sqrt{1 - \frac{X}{1 - \frac{Y^2\cos^2\theta}{2(1-X)} \pm \sqrt{\left[\frac{Y^2\cos^2\theta}{2(1-X)}\right]^2 + Y^2\sin^2\theta}}} \tag{3}$$

where, X and Y are defined using plasma frequency f_p and electron cyclotron frequency f_c, respectively, as follows:

$$X \equiv \frac{f_p^{\,2}}{f^2} \tag{4}$$

$$Y \equiv \frac{f_c}{f} \tag{5}$$

Equation (3) is a cold plasma dispersion relationship known as the Appleton-Hartree formula, and the geometrical complexity of reflective echoes appearing on an ionogram is associated with the complexity of this dispersion relationship. The double sign appearing in Equation (3) defines the refractive index of an ordinary wave (*O*-mode) when positive, and defines that of an extraordinary wave (*Z*-mode, *X*-mode) when negative. This indicates the presence of multiple propagation modes in the plasma, and for this reason, two reflective echoes appear in Fig. 1 (b). (This paper does not discuss propagations in *Z*-mode that are commonly observed in topside ionograms but rarely in bottom side ionograms. The reflection conditions for a transmitted radio wave in both *O*-mode and *X*-mode are $n = 0$, with each expressed in an equation as follows:

$$f = f_p^{\,2} \equiv f_O \tag{6}$$

$$f = \frac{f_c + \sqrt{f_c^{\,2} + 4f_p^{\,2}}}{2} \equiv f_x \tag{7}$$

where, frequencies that meet the reflection conditions for a transmitted radio wave in *O*-mode and *X*-mode are defined as f_O and f_X, respectively. Figure 3 shows the calculations of vertical height changes in V_g in both *O*-mode and *X*-mode with regard to the $N(h)$ profile shown in Fig. 2, assuming a transmitting frequency of 10 MHz. For simplicity's sake, f_c is assumed constant at 1.13 MHz. Obviously from Fig. 3, V_g is a value close to the speed of light in a low altitude region having a low electron density, but becomes lower the closer it gets to the vertical height of reflection.

In other words, the most pronounced contribution to delay time is found in the vicinity of the reflecting point. Although the $N(h)$ profile can be derived using a reflective echo in either *O*-mode or *X*-mode, the propagation mode of the reflecting echo appearing on an

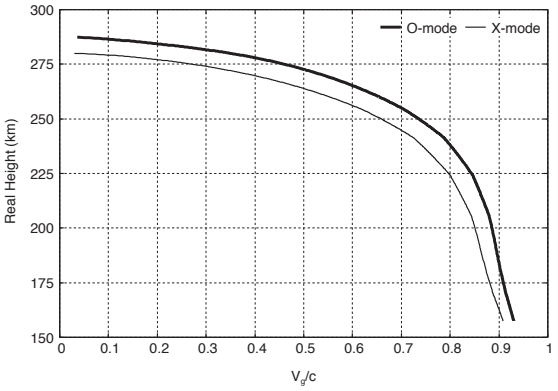

Fig.3 *Vertical height changes in V_g in O-mode and X-mode with regard to the N(h) profile shown in Fig. 2, assuming a transmitting frequency of 10 MHz.*

V_g is normalized to the speed of light c. For simplicity's sake, f_c is assumed constant at 1.13 MHz.

ionogram must be identified. In the case of ground-based ionosonde observations, *O*-mode reflective echoes are often used due to their availability with relatively high signal strength. As can be seen from Fig.1 (b), however, *O*-mode and *X*-mode reflective echoes are intricately entangled, and the delay time varies depending on the frequency. This intricate entanglement is one of the reasons for the difficulty of automatic reflective echo scaling.

3 Need to develop an automatic *O*-mode/*X*-mode tagging algorithm

Among the automatic reflective echo scaling algorithms developed to date, ARTIST4.5 (see Reference [4]) and Autoscala (see Reference [5]) focus on the work of automatically deriving $N(h)$ profiles. One of the key challenges to the task of automatically deriving $N(h)$ profiles is how to tag *O*-mode and *X*-mode reflective echoes as stated earlier. ARTIST4.5 uses ionograms on which echoes are tagged by hardware to meet this challenge. However, this algorithm is known to fail to derive $N(h)$ profiles in case of failure in the hardware-based tagging process (see Fig. 7 in Reference [7]). Moreover, considering the fact that many ionograms accumulated to date do not contain polarization information, a software implementation of tagging capability would be preferred. In contrast, Autoscala implements an algorithm whereby *O*-mode and *X*-mode reflective echoes are calculated from a predefined model $N(h)$ profile consisting of several parameters, and then compared with ionograms to find the parameters that best reproduce reflective echoes on the ionograms. It has been pointed out, however, that this algorithm fails in the automatically scaling of ionospheric reflective echoes that deviate from the predefined model profile, such as *F1.5* layer often observed in a magnetic low-latitude region [5].

Based on the limitations of existing automatic reflective echo scaling algorithms and the fact that many ionograms accumulated to date do not contain polarization information, there is a need to develop a new automatic reflective echo scaling algorithm capable of automatically tagging *O*-mode and *X*-mode reflective echoes via software, while accommodating such unusual echoes as *F1.5* layer. The development of such an algorithm requires a technique that permits the automatic tagging of *O*-mode and *X*-mode reflective echoes on an ionogram without using predefined model $N(h)$ profiles. The subsequent chapters of this paper detail the algorithm being developed for automatically tagging *O*-mode and *X*-mode reflective echoes.

4 Automatic *O*-mode/*X*-mode reflective echo tagging algorithm

As a preparatory step for tagging *O*-mode and *X*-mode reflective echoes, it is necessary to isolate reflective echoes from noise and extract reflective echo candidate points. It should be noted here that the first stage of noise removal processing should be able to retain information about reflective echoes in the vicinity of f_oF1 and f_oF2 having relatively low signal strength. Reflective echo candidate points are then extracted from residual noise in the second stage of noise removal processing to automatically tag *O*-mode and *X*-mode reflective echoes.

4.1 Noise removal processing

Figure 4 shows the workflow of the algorithm for automatically tagging *O*-mode and *X*-mode reflective echoes.

The workflow begins by calculating the average strength of individual frequencies and extracting the points having at least twice the average strength (Fig. 4 (b)). Then, the connectivity of each point (called "connectedness") defined by the following equation is calculated:

$$c(x_i,y_i)=\sum_{x(\neq x_i)}\sum_{y(\neq y_i)}\frac{1}{\sqrt{\left(x_i^{\,2}-x_j^{\,2}\right)+\left(y_i^{\,2}-y_j^{\,2}\right)}}\frac{s(x_i,y_i)s(x_j,y_j)}{1+\left|s(x_i,y_i)-s(x_j,y_j)\right|} \quad (8)$$

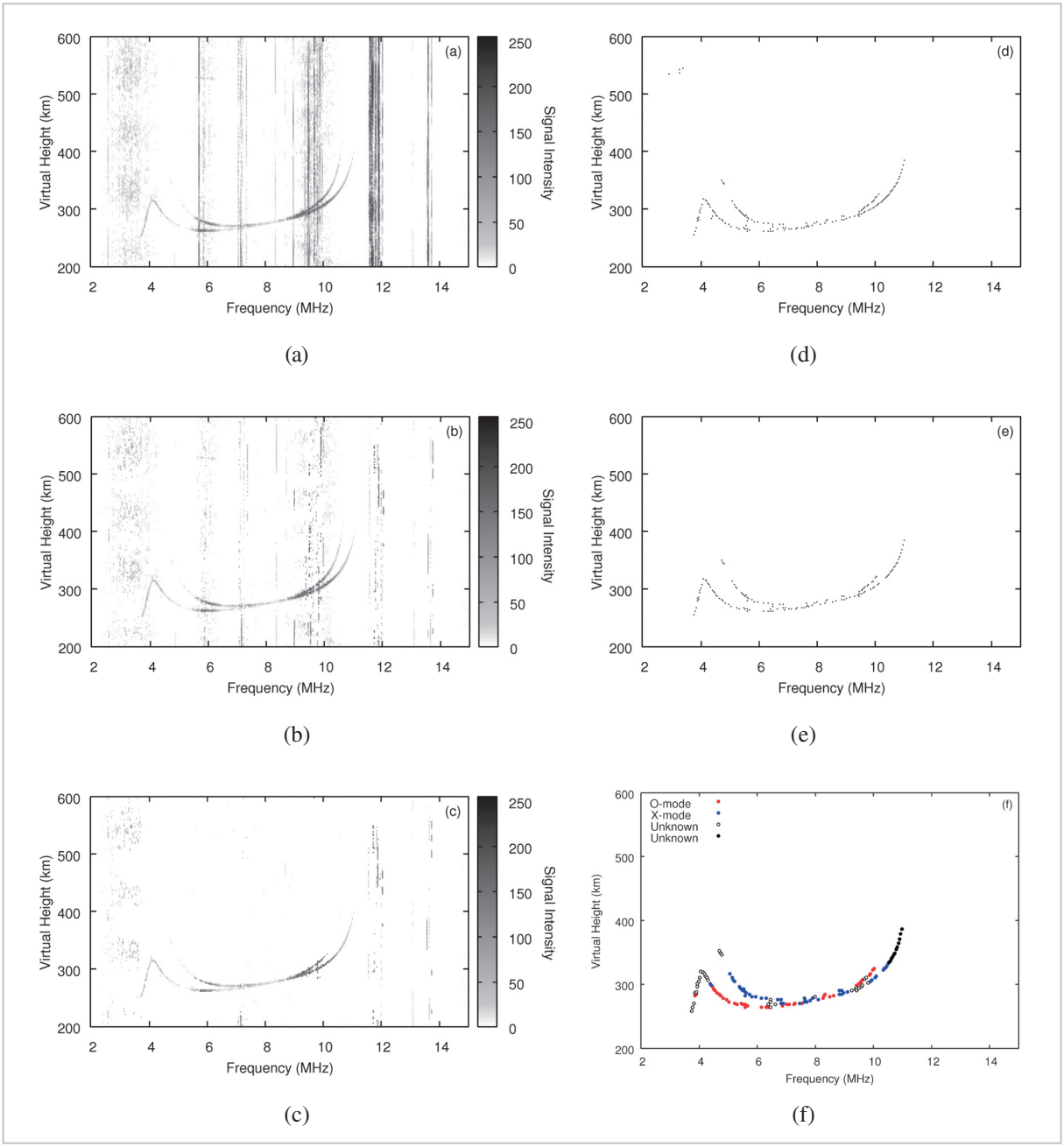

Fig.4 *Sequence of processing from noise removal processing, through extraction of reflective echo candidate points, to automatically tagging of O-mode/ and X-mode reflective echoes*

Processing proceeds from (a) to (f). Here, (a) represents a cutout portion of an ionogram collected at Chiang Mai, Thailand, at 8 UT on February 5, 2009, showing frequencies of 2 to 15 MHz and vertical heights of 200 to 600 km. The red and blue points in panel (f) designate the points tagged as being in *O*-mode (P_O) and *X*-mode (P_X), respectively, according to the automatic reflective echo scaling algorithm. Hollow points designate P_U. Each black point designates P_U higher than the maximum frequency at a point distinguished as being P_O.

where, (x_i,y_i) denote the coordinates of a pixel of interest, (x_j,y_j) any coordinates located within a certain range centering on (x_i,y_i), $c(x_i,y_i)$ the connectedness, and $s(x,y)$ the signal strength of each pixel. As can be seen from Equation (8), the higher the strength of a pixel of interest and greater the number of pixels in the vicinity having equivalent strength, the higher the value of connectedness. By evaluating the value of connectedness, reflective

echoes in the vicinity of a critical frequency having relatively a low signal strength and blurred reflective echoes, such as spread-*F*, can be kept from being omitted from noise removal processing. When many residual reflective echo candidate points left for each frequency are counted, an appropriate threshold is set on the value of connectedness calculated from Equation (8) to screen out points having a value of connectedness less than the threshold (Fig. 4 (c)). After random noise removal processing, the remaining points are thinned and binarized (Fig. 4 (d)).

4.2 Extracting reflective echo candidate points

In the second stage of processing, reflective echo candidates are extracted from the ionogram produced in the preceding stage. This stage can be considered an image processing operation that extracts multiple and arbitrary discontinuous curves from an image containing noise. Here, the technique described in Reference [8] is applied to the ionogram emerging from the first stage of processing. The technique described in Reference [8] is based on a voting process and offers the advantage of being able to extract arbitrary curves beyond reach of the Hough transform. With this technique, any two points in an image are initially selected and a likely curve is formed by selecting arbitrary points from the rest of the points in that image. Next, the validity of points that formed curve is evaluated, and the evaluated value is applied to all points that constitute the curve. The validity of the curve is evaluated based on the proximity and continuity that play a significant role in visual curve recognition. The proximity represents the degree of closeness to the distance between points. The continuity designates the smoothness of two straight lines used to interconnect three points, or how close the angle formed by the two straight lines is to 180 degrees. When the two lines shown in Fig. 5 are compared relative to their validity for example, the curve formed by the continuous line is superior in terms of proximity and continuity, and evaluated as being a more likely curve.

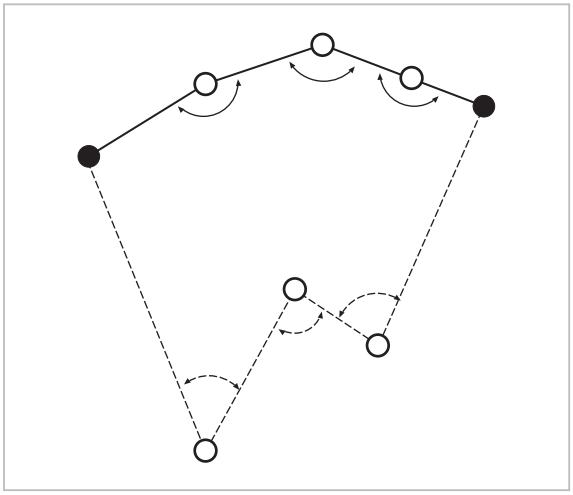

Fig.5 *Schematic view of the method of evaluating the validity of curves*

The black points denote the start and end points of a curve. Each arc with an arrow designates the interior angle formed by the two straight lines; the continuous and chain lines designate the straight lines between two points that constitute curves.

The formation of curves and the voting process are conducted for all combinations of two arbitrary points in the image to extract only the points having a high voting value as reflective echo candidate points. When this technique is applied to an ionogram, voting is conducted only on the points left after the first stage of processing, and not on all the coordinates that constitute a curve, to prevent the points at which no signal is received from being retained as curve candidates. Figure 4 (e) shows an ionogram resulting from the second stage of processing.

4.3 Automatically tagging *O*-mode/*X*-mode reflective echoes

This section describes the algorithm for automatically tagging *O*-mode and *X*-mode reflective echoes from an ionogram resulting from the second stage of processing as shown in Fig. 4 (e). Automatically tagging *O*-mode and *X*-mode reflective echoes means automatically categorizing all points left after the second stage of processing as point P_O or P_X

in *O*-mode or *X*-mode, or as point P_U if tagged as noise or otherwise unidentifiable either way. In practice, an arbitrary point *P* on an ionogram is assumed as *O*-mode point P_O. If *X*-mode point P_X associated with *O*-mode point P_O is found on the ionogram, both points are regarded as *O*-mode and *X*-mode points, respectively. Conversely, if an associated *X*-mode point is not found, the selected point *P* is assumed as P_U. The automatic tagging process is iterated for each additional point to categorize all points as being P_O, P_X, or P_U. A key to this automatic tagging process is how to calculate P_X associated with P_O. The method of calculating P_X from P_O is detailed below.

If an arbitrary point *P* is assumed as *O*-mode point P_O, transmitting frequency *f* becomes equal to the value of f_O defined by Equation (6). Thus, the arbitrary point *P* meets the reflection conditions for *O*-mode. Hence, electron density $N(h_r)$ at the reflecting point can be determined by solving Equation (6). P_O can be expressed as $P_O(f_O, h_O'(f_O))$, where $h_O'(f_O)$ can be expressed in an equation as follows:

$$h_O'(f_O) = \int_0^{h_r} n_O'(f_O, N(h), B(h), \theta(h))dh \quad (9)$$

where, n_O' denotes the *O*-mode group refractive index. To calculate n_O, the positive sign of the double sign is used in Equation (3). Evidently from the right side of Equation (9), $h_O'(f_O)$ is a function of $N(h)$ in the vertical range of vertical height h_r from the ground. (The magnetic field is calculated from a model, such as IGRF.) On the other hand, integrals in this vertical height range relating to *X*-mode propagation can be expressed by an equation like Equation (9). Transmitting frequency *f* in handling *X*-mode reflections in this integral range is frequency f_X that meets the *X*-mode reflection conditions. Since electron density $N(h_r)$ at the reflecting point is known, the value of f_X can be calculated by solving Equation (7). Although the magnetic field function is unknown in precise terms, since the difference between the actual and apparent vertical heights is on the order of up to 100 km, and is negligible compared to the earth radius of approximately 6370 km, the value from the apparent vertical height is substituted for the magnetic field function. On the basis of Equation (1), $h_X'(f_X)$ can be expressed as follows:

$$h_X'(f_X) = \int_0^{h_r} n_X'(f_X, N(h), B(h), \theta(h))dh \quad (10)$$

where, n_X' denotes the group refractive index of *X*-mode. Then, if *X*-mode point $P_X(f_X, h_X'(f_X))$ associated with point P_O can be calculated by solving Equations (9) and (10) based on the known information about point $P_O(f_O, h_O'(f_O))$ assumed as in *O*-mode, we can judge the presence or absence of the corresponding *X*-mode point on the ionogram. However, the vertical height integration on the right sides of Equations (9) and (10) cannot be solved because $N(h)$ and actual reflection vertical height h_r are unknown. This means that the calculation of point P_X associated with P_O is theoretically disabled. Hence, some assumption must be made for the purpose of approximate calculation. The fact that the group velocity of a transmitted wave propagating through plasma becomes small in the vicinity of its reflecting point as seen in Fig.3 may be utilized. This smallness suggests the integral value in the vicinity of a reflection point accounts for a great proportion of vertical height integration on the right sides of Equations (9) and (10). With this algorithm, it is therefore assumed that vertical height integration on the right sides of Equations (9) and (10) can be expressed as a constant multiple of the group refractive index in the vicinity of the reflecting point. If density N_r at the reflecting point is $N_r = N_r' + \Delta N$, Equations (9) and (10) can each be expressed as follows under this assumption:

$$h_O'(f_O) \cong \alpha n_O'(f_O, N_r', B, \theta) \quad (11)$$

$$h_X'(f_X) \cong \beta n_X'(f_X, N_r', B, \theta) \quad (12)$$

where, α and β denote coefficients relating to

the ratio of the group refractive index in the vicinity of the reflecting point to vertical height integration on the right sides of Equations (9) and (10). Because the group refractive index on the right sides of Equations (11) and (12) can be calculated analytically, when $\alpha \approx \beta$ is assumed, $hx'(f)$ can be calculated from $Po(fo,ho'(fo))$ on the basis of Equations (11) and (12) as follows under this assumption:

$$h_X'(f_X) \cong \frac{n_X'}{n_O'} h_O'(f_O) \qquad (13)$$

Using this relationship, all points are distinguished as P_O, P_X, or P_U.

Figure 6 presents a sample application of Equation (13).

The red and blue lines in Fig. 6 designate *O*-mode and *X*-mode reflective echoes that have been manually scaled from the ionogram shown in Fig. 1 (b), respectively. The pale blue line designates the *X*-mode reflective echo calculated by solving Equation (13). The calculated *X*-mode reflective echoes generally show good agreement with corresponding observations, thereby attesting to the usefulness of the automatic *O*-mode and *X*-mode tagging algorithm being discussed here.

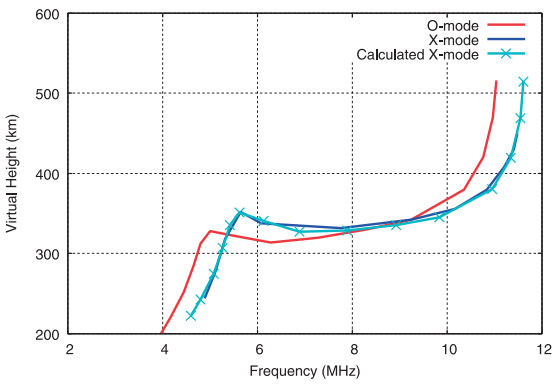

Fig.6 *Results of Eq. (13) applied to the ionogram shown in Fig. 1 (b)*

The red and blue lines designate manually scaled *O*-mode and *X*-mode reflective echoes. The check-marked pale blue line designates the *X*-mode reflective echo calculated by solving Equation (13).

Figure 4 (f) presents the results of the automatic *O*-mode and *X*-mode tagging algorithm applied to the reflective echo candidate points shown in Fig. 4 (e). The red and blue points designate the points tagged P_O and P_X by this algorithm, respectively. Hollow points designate P_U. Each black point designates P_U higher than the maximum frequency at a point distinguished as P_O. Though P_U dominates in the frequency band below $foF1$ due to the lack of *X*-mode echo, the automatic tagging process was conducted successfully.

The tagging of *O*-mode and *X*-mode alone does not yet allow us to derive an $N(h)$ profile automatically. To this end, points distinguished as P_U must be tagged as noise and P_O, since any point that should be tagged as P_O may be distinguished as P_U if *X*-mode echo voids. An algorithm for tagging as noise and P_O based on the technique discussed in Reference [9] is now being developed. Aside from this algorithm, the availability of an algorithm that can assess the reliability of automatically derived $N(h)$ profiles is also being developed. On the other hand, a set of points tagged as P_O and P_U can be regarded as an *O*-mode ionogram derived from polarization-splitting observations, although this set contains noise. Therefore, by applying ARTIST4.5 or the algorithm described in Reference [6] to *O*-mode ionograms produced by the automatic *O*-mode and *X*-mode tagging algorithm introduced in this paper, $N(h)$ profiles may be derived automatically. Further discussions should be directed at exploring the scheme of automatically deriving $N(h)$ profiles by working in conjunction with such an existing algorithm.

5 Conclusions

Achieving automatic reflective echo scaling capability forms an integral part of future sophisticated ionosonde observations, but due to the complexities of reflective echoes, existing algorithms have both merits and demerits in terms of scaling performance. In light of the limitations placed on existing automatic reflective echo scaling algorithms and the fact

that many ionograms accumulated to date do not contain polarization information, there is a need to develop a new automatic reflective echo scaling algorithm capable of automatically tagging *O*-mode and *X*-mode reflective echoes via software, while accommodating unusual reflective echoes, such as *F1.5* layer. The development of such an algorithm requires a technique that permits the automatic tagging of *O*-mode and *X*-mode reflective echoes on an ionogram without depending on a predefined model $N(h)$ profile. The automatic *O*-mode and *X*-mode tagging algorithm discussed in this paper utilizes the fact that the group velocity of a transmitted wave propagating through plasma diminishes sharply in the vicinity of its reflecting point. The algorithm makes it possible to automatically tag *O*-mode and *X*-mode reflective echoes without depending on a model $N(h)$ profile. An algorithm for automatically deriving $N(h)$ profiles from ionograms having their modes tagged by this algorithm and an algorithm for evaluating the reliability of automatically derived $N(h)$ profiles are being developed. The combined use of the automatic *O*-mode and *X*-mode tagging algorithm described in this paper with an existing algorithm such as ARTIST4.5 is also being investigated.

References

1 Alfonsi, L., G. De Franceschi, and L. Perrone, "Long term trend in the high latitude ionosphere," Physics and Chemistry of the Earth, Part C: Solar, Terrestrial & Planetary Science, vol. 26, pp. 303–307, 2001.

2 I. A. Galkin and N. I. Dvinskikh, "Interpretation of vertical incidence sounding data by electronic computing machine BECM-2M," Studies in Geomagnetism and Aeronautical Physics, vol. Sun 3, pp. 109–143, 1968.

3 M. Yoshida, "Development of an automatic ionogram processing system: 5. Automatic scaling of ionospheric parameters," Review of the Communications Research Laboratory, vol. 35, pp. 33–40, 1989.

4 B. W. Reinisch, X. Huang, I. A. Galkin, V. Paznukhov, and A. Kozlov, "Recent advances in real-time analysis of ionograms and ionospheric drift measurements with digisondes," Journal of Atmospheric and Solar-Terrestrial Physics, vol. 67, pp. 1054–1062, 2005.

5 C. Scotto, "Electron density profile calculation technique for Autoscala ionogram analysis," Advances in Space Research, vol. 44, pp. 756–766, 2009.

6 H. Kato, Y. Takiguchi, D. Fukayama, Y. Shimizu, T. Maruyama, and M. Ishii, "Development of Automatic Scaling Software of Ionospheric Parameters," Special issue of this NICT Journal, 4-1-1, 2009.

7 M. Pezzopane and C. Scotto, "Automatic scaling of critical frequency foF2 and MUF(3000)F2: A comparison between Autoscala and ARTIST 4.5 on Roma data," Radio Science, vol. 42, doi: 10.1029/2006RS003581, 2007.

8 F. Saitoh, "Curve extraction using voting process based on proximity and continuity between points", IEEJ Transactions on Electrical and Electronic Engineering, vol. 120-C, pp. 1257–1264, 2000.

9 F. Saitoh, "High speed curve extraction using genetic algorithm based on perceptive grouping factors," Journal of the Institute of Image Electronics Engineers of Japan, vol. 28, pp. 405–413, 1999.

***UEMOTO Jyunpei**, Ph.D.*

Expert Researcher, Space Enviroment Group, Applied Electromagnetic Research Center

Aeronomy

***KUBOTA Minoru**, Ph.D.*

Senior Researcher, Space Environment Group, Applied Electromagnetic Research Center

Aeronomy

***MARUYAMA Takashi**, Ph.D. (Eng.)*

Executive Researcher

Upper Atmospheric Physics

***ISHII Mamoru**, Dr. Sci.*

Director, Project Promotion Office, Applied Electromagnetic Research Center

Upper Atmospheric Physics